Strategies for Coherent Multidimensional Spectroscopy of Semiconductors

By
Blaise Jonathan Thompson

A dissertation submitted in partial fulfillment of
the requirements for the degree of

Doctor of Philosophy
(Chemistry)

at the
UNIVERSITY OF WISCONSIN - MADISON
20xx

Date of final oral examination: xx/xx/xxxx
This dissertation is approved by the following members of the Final Oral Committee:
John C. Wright, Professor, Analytical Chemistry
x
x
x
x

Contents

List of Figures **v**

List of Tables **vii**

Acknowledgments **ix**

Abstract

1 Introduction **1**

1.1 Coherent Multidimensional Spectroscopy 1

1.2 Photophysics in Semiconductor Systems 1

1.2.1 Solar Energy Generation 1

2 Spectroscopy **3**

2.1 Light 3

2.2 Light-Matter Interaction 3

2.2.1 Representations 3

2.3 Linear Spectroscopy 5

2.3.1 Reflectivity 5

2.4 Coherent Multidimensional Spectroscopy 5

2.4.1 Three Wave 5

2.4.2 Four Wave 5

2.4.3 Five Wave 5

2.4.4 Six Wave . . . 5
2.5 Strategies for CMDS . . . 6
2.5.1 Homodyne vs. Heterodyne Detection . . . 6
2.5.2 Frequency vs. Time Domain . . . 6
2.5.3 Triply Electronically Enhanced Spectroscopy . . . 7
2.5.4 Transient Absorbance Spectroscopy . . . 7
2.5.5 Cross Polarized TrEE . . . 11
2.5.6 Pump-TrEE-Probe . . . 11
2.6 Instrumental Response Function . . . 11
2.6.1 Time Domain . . . 11
2.6.2 Frequency Domain . . . 12
2.6.3 Time-Bandwidth Product . . . 13

3 Materials **15**

4 Software **17**

4.1 Overview . . . 18
4.2 WrightTools . . . 18
4.3 PyCMDS . . . 18
4.3.1 Overview . . . 18
4.3.2 Ideal Axis Positions . . . 18
4.3.3 Exponential . . . 20
4.4 WrightSim . . . 23

5 Instrumental Development **25**

5.1 Hardware . . . 25
5.1.1 Delay Stages . . . 25
5.2 Signal Acquisition . . . 25

5.2.1 Digital Signal Processing . . . 25
5.3 Artifacts and Noise . . . 25
5.3.1 Scatter . . . 25
5.4 Light Generation . . . 34
5.4.1 Automated OPA Tuning . . . 34
5.5 Optomechanics . . . 34
5.5.1 Automated Neutral Density Wheels . . . 34

6 PbSe **35**

7 MX2 **37**

8 BiVO4 **39**

A Public **41**

B Procedures **43**

C Software **45**

D Hardware **47**

D.1 Adjustable periscopes . . . 47
D.1.1 Alignment . . . 47

List of Figures

2.1 CAPTION TODO 10

4.1 TODO 22

5.1 Simulated interference paterns in old delay parameterization. 27

5.2 Simulated interference paterns in current delay parameterization. 29

5.3 Comparison of single, dual chopping. 33

List of Tables

5.1 Shot-types in phase shifted parallel modulation. 31

Acknowledgments

x

Abstract

The explanatory stories that people find compelling are simple; are concrete rather than abstract; assign a larger role to talent, stupidity and intentions than to luck; and focus on a few striking events that happened rather than on the countless events that failed to happen.

The ultimate test of an explanation is whether it would have made the event predictable in advance.

Paradoxically, it is easier to construct a coherent story when you know little, when there are fewer pieces to fit into the puzzle. Our comforting conviction that the world makes sense rests on a secure foundation: our almost unlimited ability to ignore our ignorance.

– Daniel Kahneman [1]

Chapter 1

Introduction

1.1 Coherent Multidimensional Spectroscopy

CMDS, coherent multidimensional spectroscopy

1.2 Photophysics in Semiconductor Systems

1.2.1 Solar Energy Generation

I like to do

Chapter 2

Spectroscopy

In this chapter I lay out the foundations of spectroscopy.

2.1 Light

2.2 Light-Matter Interaction

Spectroscopic experiments all derive from the interaction of light and matter. Many material properties can be deduced by measuring the nature of this interaction.

Nonlinear spectroscopy relies upon higher-order terms in the light-matter interaction. In a generic system, each term is roughly ten times smaller than the last.

2.2.1 Representations

Many strategies have been introduced for diagrammatically representing the interaction of multiple electric fields in an experiment.

Circle Diagrams

Double-sided Feynman Diagrams

WMEL Diagrams

So-called wave mixing energy level (WMEL) diagrams are the most familiar way of representing spectroscopy for Wright group members. WMEL diagrams were first proposed by Lee and Albrecht in an appendix to their seminal work *A Unified View of Raman, Resonance Raman, and Fluorescence Spectroscopy* [2]. WMEL diagrams are drawn using the following rules.

1. The energy ladder is represented with horizontal lines - solid for real states and dashed for virtual states.

2. Individual electric field interactions are represented as vertical arrows. The arrows span the distance between the initial and final state in the energy ladder.

3. The time ordering of the interactions is represented by the ordering of arrows, from left to right.

4. Ket-side interactions are represented with solid arrows.

5. Bra-side interactions are represented with dashed arrows.

6. Output is represented as a solid wavy line.

Mukamel Diagrams

2.3 Linear Spectroscopy

2.3.1 Reflectivity

This derivation adapted from *Optical Processes in Semiconductors* by Jacques I. Pankove [3]. For normal incidence, the reflection coefficient is

$$R = \frac{(n-1)^2 + k^2}{(n+1)^2 + k^2} \tag{2.1}$$

Further derivation adapted from [4]. To extend reflectivity to a differential measurement

2.4 Coherent Multidimensional Spectroscopy

multiresonant coherent multidimensional spectroscopy

2.4.1 Three Wave

2.4.2 Four Wave

Fluorescence

Raman

2.4.3 Five Wave

2.4.4 Six Wave

multiple population-period transient spectroscopy (MUPPETS)

2.5 Strategies for CMDS

2.5.1 Homodyne vs. Heterodyne Detection

Two kinds of spectroscopies: 1) heterodyne 2) homodyne. Heterodyne techniques may be self heterodyne or explicitly heterodyned with a local oscillator.

In all heterodyne spectroscopies, signal goes as N. In all homodyne spectroscopies, signal goes as N^2. This literally means that homodyne signals go as the square of heterodyne signals, which is what we mean when we say that homodyne signals are intensity level and heterodyne signals are amplitude level.

Transient absorption, TA

2.5.2 Frequency vs. Time Domain

Time domain techniques become more and more difficult when large frequency bandwidths are needed. With very short, broad pulses:

- Non-resonant signal becomes brighter relative to resonant signal
- Pulse distortions become important.

This epi-CARS paper might have some useful discussion of non-resonant vs resonant for shorter and shorter pulses [5].

An excellent discussion of pulse distortion phenomena in broadband time-domain experiments was published by Spencer et al. [6].

Another idea in defense of frequency domain is for the case of power studies. Since time-domain pulses in-fact possess all colors in them they cannot be trusted as much at perturbative fluence.

2.5.3 Triply Electronically Enhanced Spectroscopy

Triply Electronically Enhanced (TrEE) spectroscopy has become the workhorse homodyne-detected 4WM experiment in the Wright Group.

2.5.4 Transient Absorbance Spectroscopy

Transient absorption (TA)

Quantitative TA

Transient absorbance (TA) spectroscopy is a self-heterodyned technique. Through chopping you can measure nonlinearities quantitatively much easier than with homodyne detected (or explicitly heterodyned) experiments.

Figure 2.1 diagrams the TA measurement for a generic sample. Here I show measurement of both the reflected and transmitted probe beam . . . not important in opaque (pyrite) or non-reflective (quantum dot) samples . . .

Typically one attempts to calculate the change in absorbance ΔA . . .

$$\begin{aligned}
\Delta A &= A_{\text{on}} - A_{\text{off}} && (2.2)\\
&= -\log_{10}\left(\frac{I_{\text{T}} + I_{\text{R}} + I_{\Delta\text{T}} + I_{\Delta\text{R}}}{I_0}\right) + \log\left(\frac{I_{\text{T}} + I_{\text{R}}}{I_0}\right) && (2.3)\\
&= -\left(\log_{10}(I_{\text{T}} + I_{\text{R}} + I_{\Delta\text{T}} + I_{\Delta\text{R}}) - \log_{10}(I_0)\right) + \left(\log_{10}(I_{\text{T}} + I_{\text{R}}) - \log_{10}(I_0)\right) && (2.4)\\
&= -\left(\log_{10}(I_{\text{T}} + I_{\text{R}} + I_{\Delta\text{T}} + I_{\Delta\text{R}}) - \log_{10}(I_{\text{T}} + I_{\text{R}})\right) && (2.5)\\
&= -\log_{10}\left(\frac{I_{\text{T}} + I_{\text{R}} + I_{\Delta\text{T}} + I_{\Delta\text{R}}}{I_{\text{T}} + I_{\text{R}}}\right) && (2.6)
\end{aligned}$$

Equation 2.6 simplifies beautifully if reflectivity is negligible . . .

Now I define a variable for each experimental measurable:

V_{T}	voltage recorded from transmitted beam, without pump
V_{R}	voltage recorded from reflected beam, without pump
$V_{\Delta\mathrm{T}}$	change in voltage recorded from transmitted beam due to pump
$V_{\Delta\mathrm{R}}$	change in voltage recorded from reflected beam due to pump

We will need to calibrate using a sample with a known transmisivity and reflectivity constant:

$V_{\mathrm{T,\,ref}}$	voltage recorded from transmitted beam, without pump
$V_{\mathrm{R,\,ref}}$	voltage recorded from reflected beam, without pump
$\mathcal{T}_{\mathrm{ref}}$	transmissivity
$\mathcal{R}_{\mathrm{ref}}$	reflectivity

Define two new proportionality constants...

$$C_{\mathrm{T}} \equiv \frac{\mathcal{T}}{V_{\mathrm{T}}} \tag{2.7}$$

$$C_{\mathrm{R}} \equiv \frac{\mathcal{R}}{V_{\mathrm{R}}} \tag{2.8}$$

These are explicitly calibrated (as a function of probe color) prior to the experiment using the calibration sample.

Given the eight experimental measurables (V_{T}, V_{R}, $V_{\Delta\mathrm{T}}$, $V_{\Delta\mathrm{R}}$, $V_{\mathrm{T,\,ref}}$, $V_{\mathrm{R,\,ref}}$, $\mathcal{T}_{\mathrm{ref}}$, $\mathcal{R}_{\mathrm{ref}}$) I can express all of the intensities in Equation 2.6 in terms of I_0.

$$C_{\mathrm{T}} = \frac{\mathcal{T}_{\mathrm{ref}}}{V_{\mathrm{T,\,ref}}} \tag{2.9}$$

$$C_{\mathrm{R}} = \frac{\mathcal{R}_{\mathrm{ref}}}{V_{\mathrm{R,\,ref}}} \tag{2.10}$$

$$I_{\mathrm{T}} = I_0 C_{\mathrm{T}} V_{\mathrm{T}} \tag{2.11}$$

$$I_{\mathrm{R}} = I_0 C_{\mathrm{R}} V_{\mathrm{R}} \tag{2.12}$$

$$I_{\Delta\mathrm{T}} = I_0 C_{\mathrm{T}} V_{\Delta\mathrm{T}} \tag{2.13}$$

$$I_{\Delta\mathrm{R}} = I_0 C_{\mathrm{R}} V_{\Delta\mathrm{R}} \tag{2.14}$$

Wonderfully, the I_0 cancels when plugged back in to Equation 2.6, leaving a final expression for ΔA that only depends on my eight measurables.

$$\Delta A = -\log_{10}\left(\frac{C_{\mathrm{T}}(V_{\mathrm{T}} + V_{\Delta\mathrm{T}}) + C_{\mathrm{R}}(V_{\mathrm{R}} + V_{\Delta\mathrm{R}})}{C_{\mathrm{T}}V_{\mathrm{T}} + C_{\mathrm{R}}V_{\mathrm{R}}}\right) \tag{2.15}$$

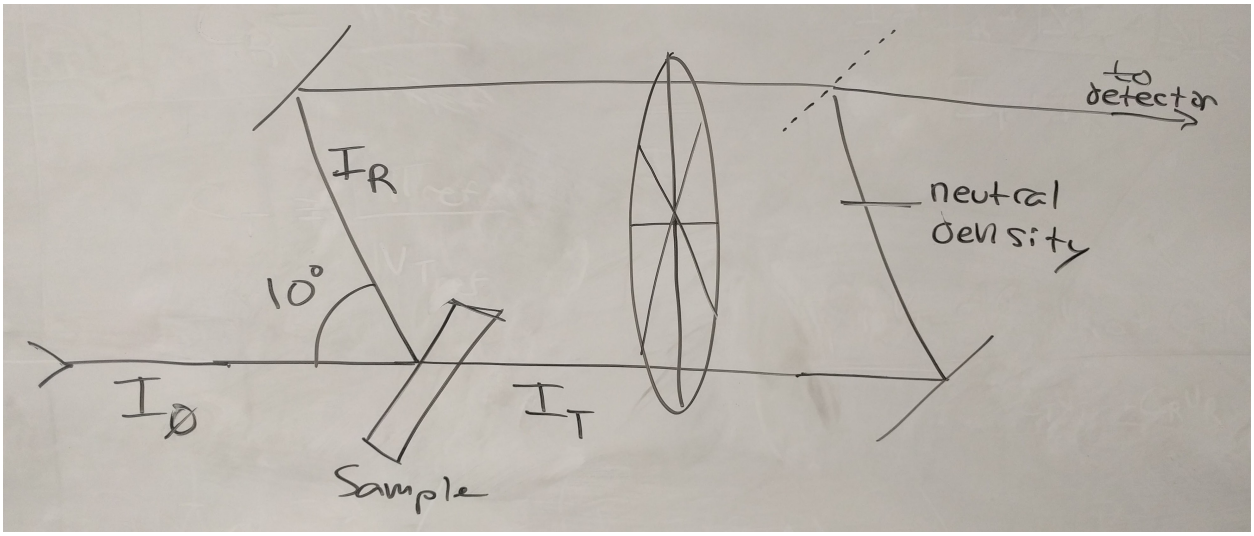

Figure 2.1: CAPTION TODO

2.5.5 Cross Polarized TrEE

2.5.6 Pump-TrEE-Probe

Pump TrEE probe (PTP).

2.6 Instrumental Response Function

The instrumental response function (IRF) is a classic concept in analytical science. Defining IRF becomes complex with instruments as complex as these, but it is still useful to attempt.

It is particularly useful to define bandwidth.

2.6.1 Time Domain

I will use four wave mixing to extract the time-domain pulse-width. I use a driven signal *e.g.* near infrared carbon tetrachloride response. I'll homodyne-detect the output. In my experiment I'm moving pulse 1 against pulses 2 and 3 (which are coincident).

The driven polarization, P, goes as the product of my input pulse *intensities*:

$$P(T) = I_1(t - T) \times I_2(t) \times I_3(t) \tag{2.16}$$

In our experiment we are convolving I_1 with $I_2 \times I_3$. Each pulse has an *intensity-level* width, σ_1, σ_2, and σ_3. $I_2 \times I_3$ is itself a Gaussian, and

$$\sigma_{I_2 I_3} = \ldots \tag{2.17}$$

$$= \sqrt{\frac{\sigma_2^2 \sigma_3^2}{\sigma_2^2 + \sigma_3^2}}. \tag{2.18}$$

The width of the polarization (across T) is therefore

$$\sigma_P = \sqrt{\sigma_1^2 + \sigma_{I_2 I_3}^2} \tag{2.19}$$

$$= \ldots \tag{2.20}$$

$$= \sqrt{\frac{\sigma_1^2 + \sigma_2^2 \sigma_3^2}{\sigma_1^2 + \sigma_2^2}}. \tag{2.21}$$

I assume that all of the pulses have the same width. I_1, I_2, and I_3 are identical Gaussian functions with FWHM σ. In this case, Equation 2.21 simplifies to

$$\sigma_P = \sqrt{\frac{\sigma^2 + \sigma^2 \sigma^2}{\sigma^2 + \sigma^2}} \tag{2.22}$$

$$= \ldots \tag{2.23}$$

$$= \sigma \sqrt{\frac{3}{2}} \tag{2.24}$$

Finally, since we measure σ_P and wish to extract σ:

$$\sigma = \sigma_P \sqrt{\frac{2}{3}} \tag{2.25}$$

Again, all of these widths are on the *intensity* level.

2.6.2 Frequency Domain

We can directly measure σ (the width on the intensity-level) in the frequency domain using a spectrometer. A tune test contains this information.

2.6.3 Time-Bandwidth Product

For a Gaussian, approximately 0.441

Chapter 3

Materials

"Kroemer's Lemma of Proven Ignorance": If, in discussing a semiconductor problem, you cannot draw an Energy Band Diagram, this shows that you don't know what you are talking about, If you can draw one, but don't, then your audience won't know what you are talking about.

Chapter 4

Software

Cutting-edge science increasingly relies on custom software. In their 2008 survey, Hannay et al. [7] demonstrated just how important software is to the modern scientist.

- → 84.3% of surveyed scientists state that developing scientific software is important or very important for their own research.
- → 91.2% of surveyed scientists state that using scientific software is important or very important for their own research.
- → On average, scientists spend approximately 40% of their work time using scientific software.
- → On average, scientists spend approximately 30% of their work time developing scientific software.

Despite the importance of software to science and scientists, most scientists are not familiar with basic software engineering concepts. This is in part due to the their general lack of formal training in programming and software development. Hannay et al. [7] found that over 90% of scientists learn software development through 'informal self study'. Indeed, I myself have never been formally trained in software development.

Software development in a scientific context poses unique challenges. Many traditional software development paradigms demand an upfront articulation of goals and requirements. This allows the developers to carefully design their software, even before a single line of code is written. In her seminal 2005 case study Segal [8] describes a collaboration between a team of researchers and a contracted team of

software engineers. Ultimately

4.1 Overview

In the Wright Group, PyCMDS replaces the old acquisition softwares 'ps control', written by Kent Meyer and 'Control for Lots of Research in Spectroscopy' written by Schuyler Kain.

4.2 WrightTools

WrightTools is a software package at the heart of all work in the Wright Group.

4.3 PyCMDS

PyCMDS directly addresses the hardware during experiments.

4.3.1 Overview

PyCMDS has, through software improvements alone, dramatically lessened scan times...

- → simultaneous motor motion
- → digital signal processing
- → ideal axis positions 4.3.2

4.3.2 Ideal Axis Positions

Frequency domain multidimensional spectroscopy is a time-intensive process. A typical pixel takes between one-half second and three seconds to acquire. Depending on the exact hardware being scanned and signal being detected, this time may be mostly due to hardware motion or signal collection. Due to the curse of dimensionality, a typical three-dimensional CMDS experiment contains roughly 100,000

pixels. CMDS hardware is transiently-reliable, so speeding up experiments is a crucial component of unlocking ever larger dimensionalities and higher resolutions.

One obvious way to decrease the scan-time is to take fewer pixels. Traditionally, multidimensional scans are done with linearly arranged points in each axis—this is the simplest configuration to program into the acquisition software. Because signal features are often sparse or slowly varying (especially so in high-dimensional scans) linear stepping means that *most of the collected pixels* are duplicates or simply noise. A more intelligent choice of axis points can capture the same nonlinear spectrum in a fraction of the total pixel count.

An ideal distribution of pixels is linearized in *signal*, not coordinate. This means that every signal level (think of a contour in the N-dimensional case) has roughly the same number of pixels defining it. If some generic multidimensional signal goes between 0 and 1, one would want roughly 10% of the pixels to be between 0.9 and 1.0, 10% between 0.8 and 0.9 and so on. If the signal is sparse in the space explored (imagine a narrow two-dimensional Lorentzian in the center of a large 2D-Frequency scan) this would place the majority of the pixels near the narrow peak feature(s), with only a few of them defining the large (in axis space) low-signal floor. In contrast linear stepping would allocate the vast majority of the pixels in the low-signal 0.0 to 0.1 region, with only a few being used to capture the narrow peak feature. Of course, linearizing pixels in signal requires prior expectations about the shape of the multidimensional signal—linear stepping is still an appropriate choice for low-resolution "survey" scans.

CMDS scans often posses correlated features in the multidimensional space. In order to capture such features as cheaply as possible, one would want to define regions of increased pixel density along the correlated (diagonal) lineshape. As a concession to reasonable simplicity, our acquisition software (PyCMDS) assumes that all scans constitute a regular array with-respect-to the scanned axes. We can acquire arbitrary points along each axis, but not for the multidimensional scan. This means that we cannot achieve strictly ideal pixel distributions for arbitrary datasets. Still, we can do much better than linear spacing.

Almost all CMDS lineshapes (in frequency and delay) can be described using just a few lineshape functions:

→ exponential

→ Gaussian

→ Lorentzian

→ bimolecular

Exponential and bimolecular dynamics fall out of simple first and second-order kinetics (I will ignore higher-order kinetics here). Gaussians come from our Gaussian pulse envelopes or from normally-distributed inhomogeneous broadening. The measured line-shapes are actually convolutions of the above. I will ignore the convolution except for a few illustrative special cases. More exotic lineshapes are possible in CMDS—quantum beating and breathing modes, for example—I will also ignore these. Derivations of the ideal pixel positions for each of these lineshapes appear below.

4.3.3 Exponential

Simple exponential decays are typically used to describe population and coherence-level dynamics in CMDS. For some generic exponential signal S with time constant τ,

$$S(t) = \mathrm{e}^{-\frac{t}{\tau}}. \tag{4.1}$$

We can write the conjugate equation to 4.1, asking "what t do I need to get a certain signal level?":

$$\log(S) = -\frac{t}{\tau} \tag{4.2}$$

$$t = -\tau \log(S). \tag{4.3}$$

So to step linearly in t, my step size has to go as $-\tau \log(S)$.

We want to go linearly in signal, meaning that we want to divide S into even sections. If S goes from 0 to 1 and we choose to acquire N points,

$$t_n = -\tau \log\left(\frac{n}{N}\right). \tag{4.4}$$

Note that t_n starts at long times and approaches zero delay. So the first t_1 is the smallest signal and t_N is the largest.

Now we can start to consider realistic cases, like where τ is not quite known and where some other longer dynamics persist (manifested as a static offset). Since these values are not separable in a general system, I'll keep S normalized between 0 and 1.

$$S = (1-c)\,\mathrm{e}^{-\frac{t}{\tau_{\text{actual}}}} + c \tag{4.5}$$

$$S_n = (1-c)\,\mathrm{e}^{-\frac{-\tau_{\text{step}} \log\left(\frac{n}{N}\right)}{\tau_{\text{actual}}}} + c \tag{4.6}$$

$$S_n = (1-c)\,\mathrm{e}^{-\frac{\tau_{\text{step}}}{\tau_{\text{actual}}} \log\left(\frac{N}{n}\right)} + c \tag{4.7}$$

$$S_n = (1-c)\left(\frac{N}{n}\right)^{-\frac{\tau_{\text{step}}}{\tau_{\text{actual}}}} + c \tag{4.8}$$

$$S_n = (1-c)\left(\frac{n}{N}\right)^{\frac{\tau_{\text{step}}}{\tau_{\text{actual}}}} + c \tag{4.9}$$

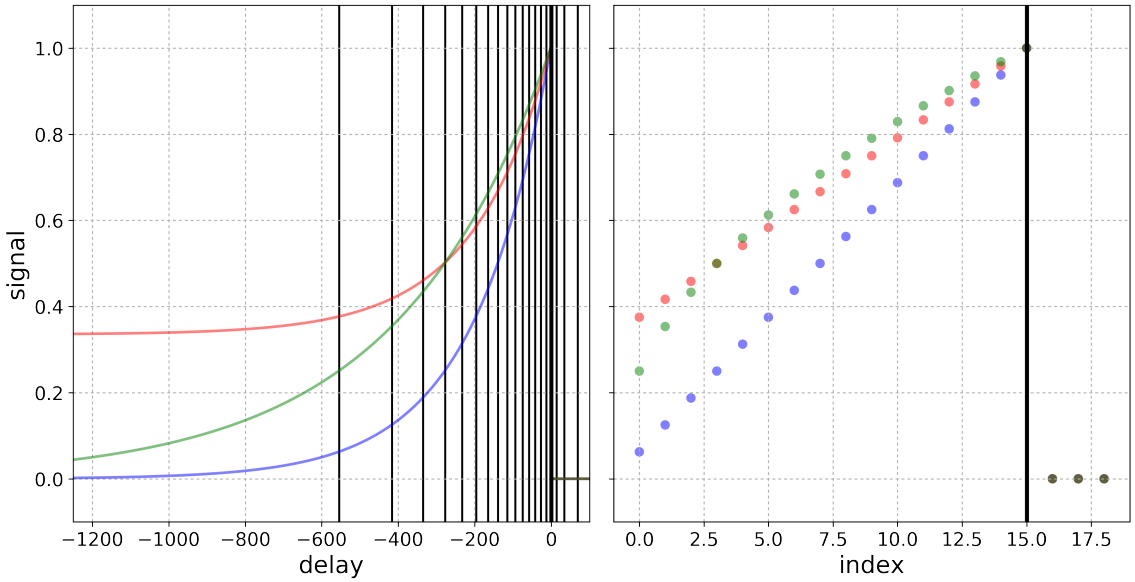

Figure 4.1: TODO

Gaussian

Lorentzian

Bimolecular

4.4 WrightSim

WrightSim does simulations.

Chapter 5

Instrumental Development

5.1 Hardware

5.1.1 Delay Stages

5.2 Signal Acquisition

Old boxcar: 300 ns window, 10 micosecond delay. Onset of saturation 2 V.

5.2.1 Digital Signal Processing

5.3 Artifacts and Noise

5.3.1 Scatter

Scatter is a complex microscopic process whereby light traveling through a material elastically changes its propagation direction. In CMDS we use propagation direction to isolate signal. Scattering samples defeat this isolation step and allow some amount of excitation light to reach the detector. In homodyne-

detected 4WM experiments,

$$I_{\text{detected}} = |E_{4\text{WM}} + E_1 + E_2 + E_{2'}|^2 \tag{5.1}$$

Where E is the entire time-dependent complex electromagnetic field. When expanded, the intensity will be composed of diagonal and cross terms:

$$\begin{aligned} I_{\text{detected}} = \overline{(E_1 + E_2)}E_{2'} + (E_1 + E_2)\overline{E_{2'}} + |E_1 + E_2|^2 + (E_1 + E_2)\overline{E_{4\text{WM}}} \\ +(E_1 + E_2)\overline{E_{4\text{WM}}} + \overline{E_{2'}}E_{4\text{WM}} + E_{2'}\overline{E_{4\text{WM}}} + |E_{4\text{WM}}|^2 \end{aligned} \tag{5.2}$$

A similar expression in the case of heterodyne-detected 4WM is derived by Brixner et al. [9]. The goal of any 'scatter rejection' processing procedure is to isolate $|E_{4\text{WM}}|^2$ from the other terms.

Abandon the Random Phase Approximation

Interference Patterns in TrEE

TrEE is implicitly homodyne-detected. Scatter from excitation fields will interfere on the amplitude level with TrEE signal, causing interference patterns that beat in delay and frequency space. The pattern of beating will depend on which excitation field(s) reach(es) the detector, and the parameterization of delay space chosen.

First I focus on the interference patterns in 2D delay space where all excitation fields and the detection field are at the same frequency.

Here I derive the slopes of constant phase for the old delay space, where d1 = $\tau_{2'1}$ and d2 = τ_{21}. For simplicity, I take τ_1 to be 0, so that $\tau_{21} \rightarrow \tau_2$ and $\tau_{2'1} \rightarrow \tau_{2'}$. The phase of signal is then

$$\Phi_{\text{sig}} = \mathrm{e}^{-((\tau_{2'} - \tau_2)\omega)} \tag{5.3}$$

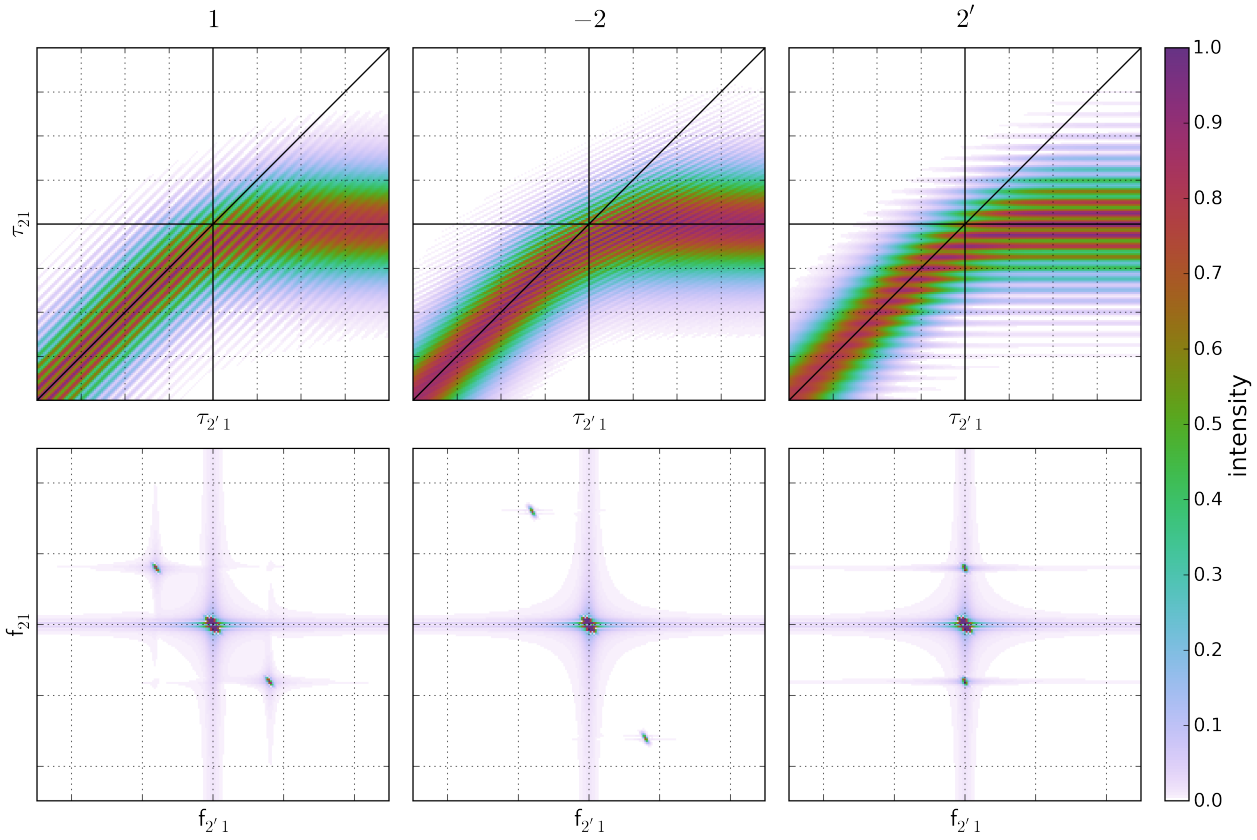

Figure 5.1: Numerically simulated interference patterns between scatter and TrEE for the old delay parametrization. Each column has scatter from a single excitation field. The top row shows the measured intensities, the bottom row shows the 2D Fourier transform, with the colorbar's dynamic range chosen to show the cross peaks.

The phase of each excitation field can also be written:

$$\Phi_1 = e^0 \tag{5.4}$$

$$\Phi_2 = e^{-\tau_2 \omega} \tag{5.5}$$

$$\Phi_{2'} = e^{-\tau_{2'} \omega} \tag{5.6}$$

The cross term between scatter and signal is the product of Φ_{sig} and $\Phi_{scatter}$. The cross terms are:

$$\Delta_1 = \Phi_{sig} = e^{-((\tau_{2'} - \tau_2)\omega)} \tag{5.7}$$

$$\Delta_2 = \Phi_{sig} e^{-\tau_2 \omega} = e^{-((\tau_{2'} - 2\tau_2)\omega)} \tag{5.8}$$

$$\Delta_{2'} = \Phi_{sig} e^{-\tau_{2'} \omega} = e^{-\tau_2 \omega} \tag{5.9}$$

Figure 5.1 presents numerical simulations of scatter interference as a visual aid. See Yurs 2011 [10].

Here I derive the slopes of constant phase for the current delay space, where d1 = $\tau_{22'}$ and d2 = τ_{21}. I take τ_2 to be 0, so that $\tau_{22'} \rightarrow \tau_{2'}$ and $\tau_{21} \rightarrow \tau_1$. The phase of the signal is then

$$\Phi_{sig} = e^{-((\tau_{2'} + \tau_1)\omega)} \tag{5.10}$$

The phase of each excitation field can also be written:

$$\Phi_1 = e^{-\tau_1 \omega} \tag{5.11}$$

$$\Phi_2 = e^0 \tag{5.12}$$

$$\Phi_{2'} = e^{-\tau_{2'} \omega} \tag{5.13}$$

The cross term between scatter and signal is the product of Φ_{sig} and $\Phi_{scatter}$. The cross terms are:

$$\Delta_1 = \Phi_{sig} e^{-\tau_1 \omega} = e^{-\tau_{2'} \omega} \tag{5.14}$$

$$\Delta_2 = \Phi_{sig} = e^{-((\tau_2 + \tau_1)\omega)} \tag{5.15}$$

$$\Delta_{2'} = \Phi_{sig} e^{-\tau_{2'} \omega} = e^{-\tau_1 \omega} \tag{5.16}$$

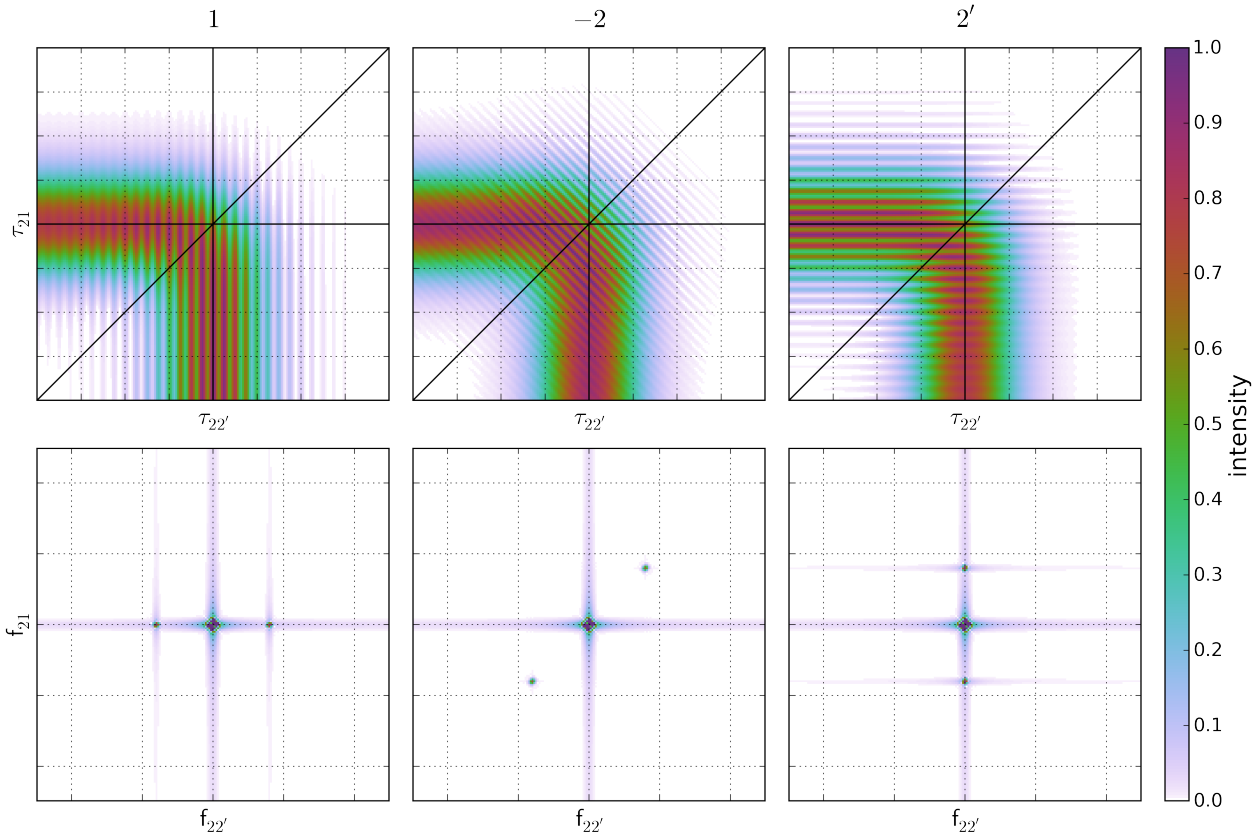

Figure 5.2: Numerically simulated interference patterns between scatter and TrEE for the current delay parametrization. Each column has scatter from a single excitation field. The top row shows the measured intensities, the bottom row shows the 2D Fourier transform, with the colorbar's dynamic range chosen to show the cross peaks.

Figure 5.2 presents numerical simulations of scatter interference for the current delay parameterization.

Instrumental Removal of Scatter

The effects of scatter can be entirely removed from CMDS signal by combining two relatively straightforward instrumental techniques: *chopping* and *fibrillation*. Conceptually, chopping removes intensity-level offset terms and fibrillation removes amplitude-level interference terms. Both techniques work by modulating signal and scatter terms differently so that they may be separated after light collection.

	A	B	C	D
signal			✓	
scatter 1		✓	✓	
scatter 2			✓	✓
other	✓	✓	✓	✓

Table 5.1: Four shot-types in a general phase shifted parallel modulation scheme. The 'other' category represents anything that doesn't depend on either chopper, including scatter from other excitation sources, background light, detector voltage offsets, etc.

We use the dual chopping scheme developed by Furuta, Fuyuki, and Wada [11] called 'phase shifted parallel modulation'. In this scheme, two excitation sources are chopped at 1/4 of the laser repetition rate (two pulses on, two pulses off). Very similar schemes are discussed by Augulis and Zigmantas [12] and Heisler et al. [13] for two-dimensional electronic spectroscopy. The two chop patterns are phase-shifted to make the four-pulse pattern represented in Table 5.1. In principle this chopping scheme can be achieved with a single judiciously placed mechanical chopper - this is one of the advantages of Furuta's scheme. Due to practical considerations we have generally used two choppers, one on each OPA. The key to phase shifted parallel modulation is that signal only appears when both of your chopped beams are passed. It is simple to show how signal can be separated through simple addition and subtraction of the A, B, C, and D phases shown in Table 5.1. First, the components of each phase:

$$A = I_{\text{other}} \tag{5.17}$$

$$B = I_1 + I_{\text{other}} \tag{5.18}$$

$$C = I_{\text{signal}} + I_1 + I_2 + I_{\text{other}} \tag{5.19}$$

$$D = I_2 + I_{\text{other}} \tag{5.20}$$

Grouping into difference pairs,

$$A - B = -I_1 \tag{5.21}$$

$$C - D = I_{\text{signal}} + I_1 \tag{5.22}$$

So:

$$A - B + C - D = I_{\text{signal}} \tag{5.23}$$

I have ignored amplitude-level interference terms in this treatment because they cannot be removed via any chopping strategy. Interference between signal and an excitation beam will only appear in 'C'-type shots, so it will not be removed in Equation 5.23. To remove such interference terms, you must *fibrillate* your excitation fields.

An alternative to dual chopping is single-chopping and 'leveling'... this technique was used prior to May 2016 in the Wright Group... 'leveling' and single-chopping is also used in some early 2DES work... [9].

Figure 5.3 shows the effects of dual chopping for some representative MoS_2 TA data. Each subplot is a probe wigner, with the vertical grey line representing the pump energy. Note that the single chopper passes pump scatter, visible as a time-invariant increase in intensity when the probe and monochromator are near the pump energy. Dual chopping efficiently removes pump scatter, but at the cost of signal to noise for the same number of laser shots. Taking twice as many laser shots when dual chopping brings the signal to noise to at least as good as the original single chopping.

Fibrillation is the intentional randomization of excitation phase during an experiment. Because the interference term depends on the phase of the excitation field relative to the signal, averaging over many shots with random phase will cause the interference term to approach zero. This is a well known strategy for removing unwanted interference terms [14, 15].

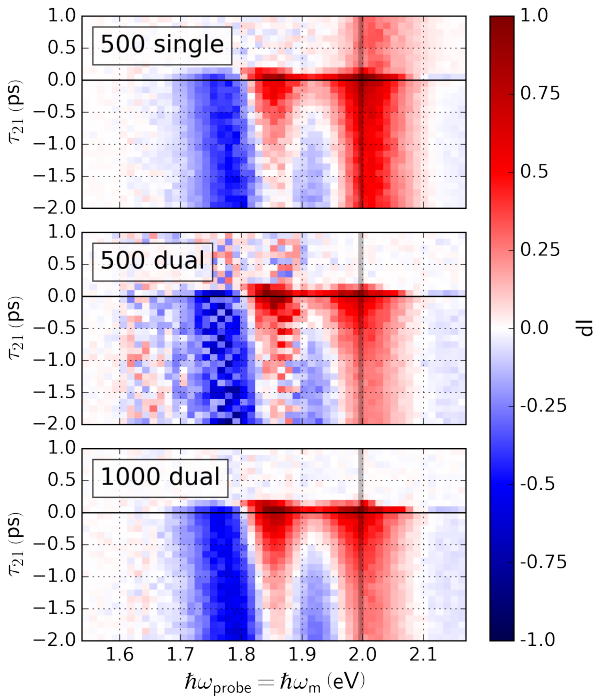

Figure 5.3: Comparison of single and dual chopping in a MoS_2 transient absorption experiment. Note that this data has not been processed in any way - the colorbar represents changes in intensity seen by the detector. The grey line near 2 eV represents the pump energy. The inset labels are the number of laser shots taken and the chopping strategy used.

5.4 Light Generation

5.4.1 Automated OPA Tuning

5.5 Optomechanics

5.5.1 Automated Neutral Density Wheels

Chapter 6

PbSe

Chapter 7

MX2

Chapter 8

BiVO4

Appendix A

Public

A.1 Why spectroscopy?

A.2 CMDS in practice

A.2.1 Ultrafast light sources

Appendix B

Procedures

Appendix C

Software

Appendix D

Hardware

D.1 Adjustable periscopes

Our light sources take on horizontal or vertical polarizations according to which tuning process is used. Our experiments are opinionated about polarization, so some strategy for aligning polarization is necessary. Desire fully reflective, easy to switch without changing path length (delay) etc... For several years, we used brewster-angle polarization unifiers... These worked by... But these were very difficult to align, and they were too lossy for some of the weaker tuning processes. As an alternative, we designed a more traditional periscope with adjustability for our unique needs.

D.1.1 Alignment

1. in flipped polarization:
    - stage near
    - upper mirror far
2. in kept polarization:
    - stage x and upper mirror height near
    - lower mirror far

Bibliography

[1] Daniel Kahneman. *Thinking, Fast and Slow*. Farrar, Straus and Giroux, 2013. ISBN: 9780374533557.

[2] Duckhwan Lee and Andreas C. Albrecht. "A Unified View of Raman, Resonance Raman, and Fluorescence Spectroscopy (and their Analogues in Two-Photon Absorption". In: *Advances in infrared and Raman Spectroscopy*. Ed. by R. J. H. Clark and R. E. Hester. 1st ed. London; New York, 1985. Chap. 4, pp. 179–213. ISBN: 9780471906742.

[3] Jacques Pankove. *Optical Processes in Semiconductors*. Dover Publications, 1975. ISBN: 9780486602752.

[4] Nardeep Kumar, Jiaqi He, Dawei He, Yongsheng Wang, and Hui Zhao. "Charge carrier dynamics in bulk MoS2 crystal studied by transient absorption microscopy". In: *Journal of Applied Physics* 113.13 (2013), p. 133702. DOI: 10.1063/1.4799110.

[5] Ji-xin Cheng, Andreas Volkmer, Lewis D Book, and X Sunney Xie. "An Epi-Detected Coherent Anti-Stokes Raman Scattering (E-CARS) Microscope with High Spectral Resolution and High Sensitivity". In: *The Journal of Physical Chemistry B* 105.7 (Feb. 2001), pp. 1277–1280. DOI: 10.1021/jp003774a.

[6] Austin P. Spencer, Hebin Li, Steven T. Cundiff, and David M. Jonas. "Pulse Propagation Effects in Optical 2D Fourier-Transform Spectroscopy: Theory". In: *The Journal of Physical Chemistry A* 119.17 (2015), pp. 3936–3960. DOI: 10.1021/acs.jpca.5b00001.

[7] Jo Erskine Hannay, Carolyn MacLeod, Janice Singer, Hans Petter Langtangen, Dietmar Pfahl, and Greg Wilson. "How do scientists develop and use scientific software?" In: *2009 ICSE Workshop on Software Engineering for Computational Science and Engineering*. Institute of Electrical and Electronics Engineers (IEEE), May 2009. DOI: 10.1109/secse.2009.5069155.

[8] Judith Segal. "When Software Engineers Met Research Scientists: A Case Study". In: *Empirical Software Engineering* 10.4 (Oct. 2005), pp. 517–536. DOI: 10.1007/s10664-005-3865-y.

[9] Tobias Brixner, Tomas Mancal, Igor V. Stiopkin, and Graham R. Fleming. "Phase-stabilized two-dimensional electronic spectroscopy". In: *The Journal of Chemical Physics* 121.9 (2004), p. 4221. DOI: 10.1063/1.1776112.

[10] Lena A Yurs, Stephen B. Block, Andrei V Pakoulev, Rachel S. Selinsky, Song Jin, and John Wright. "Multiresonant Coherent Multidimensional Electronic Spectroscopy of Colloidal PbSe Quantum Dots". In: *The Journal of Physical Chemistry C* 115.46 (Nov. 2011), pp. 22833–22844. DOI: 10.1021/jp207273x.

[11] Koichi Furuta, Masanori Fuyuki, and Akihide Wada. "Cross-Term Selective, Two-Pulse Correlation Measurements by Phase-Shifted Parallel Modulation for Analysis of a Multi-Photon Process". In: *Applied Spectroscopy* 66.12 (Dec. 2012), pp. 1475–1479. DOI: 10.1366/12-06657.

[12] Ramūnas Augulis and Donatas Zigmantas. "Two-dimensional electronic spectroscopy with double modulation lock-in detection: enhancement of sensitivity and noise resistance." In: *Optics express* 19.14 (June 2011), pp. 13126–13133. DOI: 10.1364/OE.19.013126.

[13] Ismael A. Heisler, Roberta Moca, Franco V A Camargo, and Stephen R. Meech. "Two-dimensional electronic spectroscopy based on conventional optics and fast dual chopper data acquisition". In: *Review of Scientific Instruments* 85.6 (June 2014), p. 063103. DOI: 10.1063/1.4879822.

[14] Ivan C. Spector, Courtney M. Olson, Christopher J. Huber, and Aaron M. Massari. "Simple fully reflective method of scatter reduction in 2D-IR spectroscopy". In: *Optics Letters* 40.8 (Apr. 2015), pp. 1850–1852. DOI: 10.1364/OL.40.001850.

[15] Brian L. McClain, Ilya J. Finkelstein, and M. D. Fayer. "Vibrational echo experiments on red blood cells: Comparison of the dynamics of cytoplasmic and aqueous hemoglobin". In: *Chemical Physics Letters* 392.4-6 (July 2004), pp. 324–329. DOI: 10.1016/j.cplett.2004.05.080.